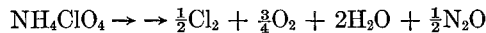


Fig 2 Schematic of heterogeneous reactions occurring at oxidizer particle-polymeric binder interface

steep temperature gradient is established in the solid. This gradient extends to a depth of several microns, depending upon the external heat-flux rate. As the propellant surface layers approach  $150^{\circ}\text{C}$ , the intermosaic blocks of the oxidizer particles<sup>8</sup> decompose, and gaseous products diffuse to the oxidizer particle-fuel interface. From ammonium perchlorate decomposition studies, the over-all reaction for the low-temperature decomposition has been shown to be<sup>9</sup>



Thus, oxidizing gases are generated at the propellant surface and in the surface layers from decomposition of the solid oxidizer, as shown schematically in Fig 2. Under these conditions, oxidizing species react heterogeneously with the adjacent fuel to generate a source of heat. Once these reactions reach runaway conditions, ignition has been achieved. Hence, the heterogeneous reactions between the oxidizer decomposition products and the fuel control the internal response of the propellant to the external heat flux.

The model explains the observed effects on the ignition delay time of heat flux, pressure, initial temperature, and catalyst content. Although the description herein has been made for composite propellants that contain ammonium perchlorate, it is completely general and applies to all composite and double-base propellants. Details of the theory and confirming experimental evidence will be presented in a subsequent publication.<sup>10</sup>

#### Role of Heterogeneous Reactions in Solid Propellant Combustion

The temperature and pressure during steady-state combustion are significantly higher than required for these heterogeneous reactions to reach runaway conditions. Consequently, these reactions can play a dominant role in the over-all deflagration process and have been shown to explain a number of observed effects not incorporated in gas-phase combustion theories. For example, the diffusion flame theory does not predict the high burning rate nor large pressure exponents of burning rate that are observed with composite propellants containing potassium and lithium perchlorate. When these metal salts are used instead of ammonium perchlorate, the heterogeneous reaction is greatly enhanced by an increase of reactive oxidizer species from oxidizer decomposition. The  $\text{KClO}_4$  and  $\text{LiClO}_4$  decomposition generates a much higher concentration of oxidizer gases than for  $\text{NH}_4\text{ClO}_4$ , since  $\text{NH}_3$ ,  $\text{H}_2\text{O}$ , and other fuel-based species are absent. For these oxidizers, the heterogeneous reactions have been observed to exhibit a more dominant role, which explains the apparently anomalous pressure and burning-rate behavior. Experimental and theoretical evidence in support of the theory will be presented in a subsequent publication.<sup>11</sup>

Therefore, heterogeneous reactions coupled with gas-phase reactions provide clear insight into the several unit proc-

esses that control the burning rate of solid propellants and related phenomena, such as combustion termination. In addition, this model provides a possible means of coupling the over-all combustion process with oscillatory acoustical phenomena.

#### References

- Anderson, R., Ignition research sponsored by Bur Naval Weapons at United Technology Center (1962-1963)
- Brown, R. S., ignition research sponsored by NASA at United Technology Center (1962-1963)
- Fullman, C. H. and Nielsen, F. B., ignition research sponsored by U. S. Air Force at United Technology Center (1961-1963)
- Anderson, R. and Brown, R. S., "Ignition of solid propellants," U. S. Air Force Office Sci. Res. Contractors Meeting, Silver Spring, Md. (March 6, 1963)
- McAlevy, R. F. and Summerfield, M., "The ignition mechanism of composite solid propellants," Final Rept., Contract U. S. Air Force OSRA 49(630)-411 (June 1, 1961)
- Allen, H., Jr. and Pinns, M. L., "Relative ignitability of typical solid propellants with chlorine trifluoride," NASA TN D-1533 (January 1963)
- Anderson, R., Brown, R. S., Thompson, G. T., and Ebeling, R. W., "Fundamental investigation on hypergolic ignition for solid propellants," AIAA Conference on Heterogeneous Combustion, Palm Beach, Fla. (December 1963)
- Galwey, A. K. and Jacobs, P. W. M., "The thermal decomposition of ammonium perchlorate at low temperature," Proc. Roy. Soc. (London) A254, 455-469 (1960)
- Bircumshaw, L. L. and Newman, B. H., "The thermal decomposition of ammonium perchlorate," Proc. Roy. Soc. (London) A227, 115-132 (1954); also A227, 228-241 (1955)
- Anderson, R., Brown, R. W., and Shannon, L. J., "Heterogeneous reaction ignition theory of solid propellants," AIAA Solid Propellant Rocket Conference, Palo Alto, Calif. (January 1964)
- Anderson, R., Brown, R. S., and Shannon, L. J., "Fundamental mechanisms of solid-propellant combustion" (in preparation)

## Effect of the Boundary Layer upon the Flow in a Conical Hypersonic Nozzle

MARTIN SICHEL\*

University of Michigan, Ann Arbor, Mich

#### Nomenclature

$Re_x$	= Reynolds number based on nozzle length
$x$	= distance from throat to nozzle exit
$R, r_t$	= nozzle and throat radius
$M$	= Mach number
$\rho_R$	= reference density at standard conditions = $8.042 \times 10^{-2}$ lb/ft <sup>3</sup>
$\theta_w$	= nozzle half angle
$A_{geom}, A_t$	= geometric and throat area of the nozzle

IN hypersonic wind-tunnel nozzles the boundary layer may occupy as much as 50% of the test section area<sup>1</sup> and so exerts a major influence upon the flow. An application of a method developed by Burke and Bird<sup>2</sup> to the calculation of the combined core/boundary-layer flow in a conical hypersonic nozzle over a broad range of stagnation conditions has brought to light some surprising results, which are reported below.

Received November 4, 1963. The work reported here was sponsored by the Office of Naval Research under Contract Nonr-1224(31), NR 061-108.

\* Assistant Professor, Department of Aeronautical and Astronautical Engineering. Member AIAA.

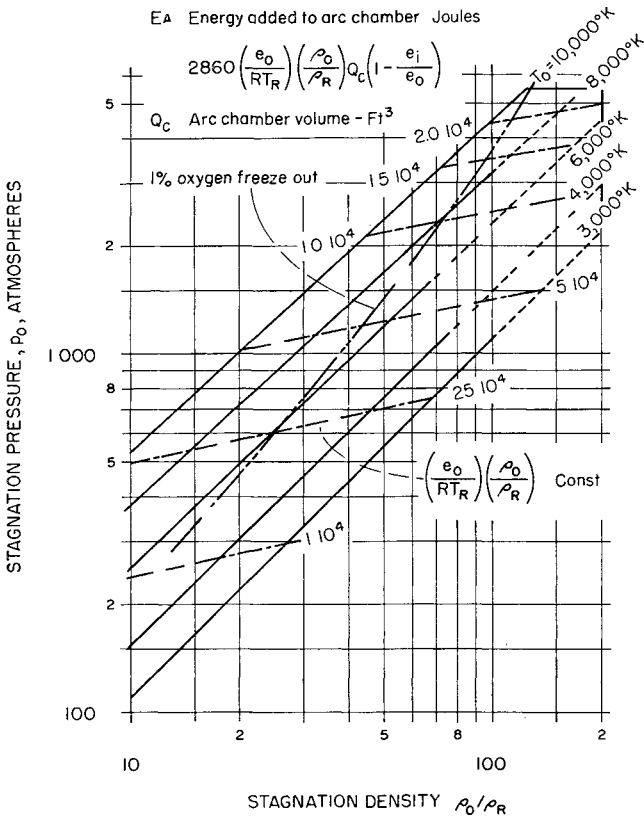


Fig 1 Arc chamber conditions for equilibrium air

Burke and Bird<sup>2</sup> sidestep the solution of the boundary-layer integral equations along the nozzle by using either the empirical relation

$$\delta_1/x = KM_e^a/Re_x^b \quad (1)$$

or the relation

$$\delta_1/x = \bar{K}(\rho^*u_e x/\mu^*)^{-\lambda} \quad (2)$$

for the displacement thickness  $\delta_1$  at the nozzle exit. The asterisk refers to quantities evaluated at the Eckert reference temperature.<sup>3</sup> Consideration of experimental results covering the range  $1.5 \times 10^5 \leq Re_x \leq 8 \times 10^6$  suggested the values  $\bar{K} = 0.49$ ,  $\lambda = 0.3$  for the empirical constants in Eq (2). By combining Eq (2) with the continuity equation

$$\dot{m} = \pi \rho_e u_e (R - \delta_1)^2 \quad (3)$$

Burke and Bird showed that the ratio of the displacement thickness to the nozzle radius  $R = \theta_w x$  satisfies the equation

$$\delta_1/R = \mathcal{G}[1 - (\delta_1/R)]^{2\gamma\lambda} F_2(p_0, h_0) \quad (4)$$

$\mathcal{G}$  is a geometrical factor given by

$$\mathcal{G} = \frac{1}{\theta_w x^\lambda} \left(\frac{\theta_w x}{r_t}\right)^{2\gamma\lambda} = \frac{1}{\theta_w x^\lambda} \left(\frac{A_{geom}}{A_t}\right)^{\gamma\lambda} = \left(\frac{x}{R}\right) \left(\frac{R}{r_t}\right)^{2\gamma\lambda} x^{-\lambda} \quad (5)$$

The calculation of  $F_2(p_0, h_0)$ , which is a function only of the stagnation pressure and enthalpy, depends upon the assumptions that the nozzle flow is in chemical equilibrium everywhere, and that the perfect gas assumption is valid in the freestream so that the approximate nozzle flow equations of Reece<sup>4</sup> are applicable. The details of these calculations are presented in Ref 5. Reece's method was also used to calculate other core flow parameters.

The thermodynamic data for air from Refs 6-8 was used in the calculations. Results for  $\rho_0/\rho_R > 100$  were obtained by extrapolating the air Mollier diagram and so must be re-

garded with considerable caution. Although data for argon-free air and the more recent data for air including argon were used interchangeably, the effects of this inconsistency can be ignored in view of the large uncertainty introduced by the empirical displacement thickness formula. All results are presented as curves on stagnation pressure-density diagrams, a form of presentation which is especially convenient for hot-shot or arc-discharge tunnels.

The range of stagnation conditions considered is indicated in Fig 1, which also shows curves of constant stagnation temperature  $T_0$  and dimensionless energy per unit volume  $(e_0/RT_R)(\rho_0/\rho_R)$ . The results presented by Lukasiewicz<sup>9</sup> have been used to compute a curve in Fig 1 corresponding to the case in which 1% of the oxygen in the air freezes out in atomic form. The equilibrium assumption should be valid below the 1% freeze-out curve, and indications are that oxygen freeze-out will not exceed 10% over the range of stagnation conditions considered here.

Contours of constant values of the ratio of displacement thickness to test section radius  $\delta_1/R$  are shown in Fig 2. Unfortunately the results could not be generalized, and in the present case they are valid only for the particular value  $\mathcal{G} = 363 \text{ ft}^{-0.3}$  of the geometrical factor corresponding, for example, to  $\theta_w = 7.5^\circ$ ,  $r_t = 0.05 \text{ in}$ ,  $x = 72.0 \text{ in}$ ,  $\lambda = 0.3$  ( $\delta_1/R$ ) decreases with increasing stagnation pressure, which is not surprising. What is remarkable is that the curves in Fig 2 pass through a maximum, which means that, for constant stagnation pressure  $p_0$ , as the stagnation density  $\rho_0$  increases, the boundary-layer thickness at first increases and then begins to decrease. Consideration of the displacement thickness correlation formula, Eq (1), and Fig 3, which shows contours of constant test section Mach number, provides an explanation for this strange result. With  $p_0$  constant, an increase in  $\rho_0$  causes the test section Mach number to increase, and this in turn tends to increase  $\delta_1$ . On the other hand, the static density and Reynolds number also increase, and this has the opposite effect. The maxi-

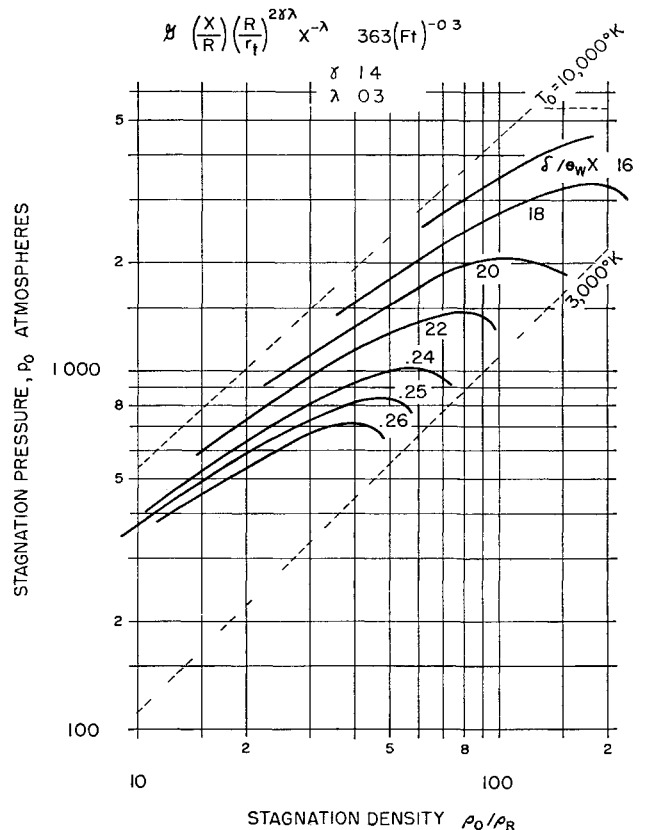


Fig 2 Variation of test section boundary-layer thickness with stagnation conditions

imum in the boundary-layer contours in Fig 2 thus corresponds to the point where these opposing effects balance

The presence of the boundary layer has a very strong effect upon the test section static pressure and density as can, for example, be seen from Fig 4, which shows test section densities both with and without consideration of the boundary layer. In the present case the presence of the boundary layer almost doubles the freestream density and static pressure. On the other hand, since in hypersonic flow  $u_e \cong (2h_0)^{1/2}$ , the freestream velocity is essentially independent of boundary-layer development

Reece's<sup>4</sup> approximate nozzle flow equations are accurate to 1% for  $T < 550^\circ\text{K}$ , and according to Fig 5, which shows curves of constant test section static temperature, they should remain valid over most of the stagnation range considered here. In the present case the freestream Reynolds number lies in the range  $0.4 \times 10^5 \leq Re_x \leq 4 \times 10^6$ , which almost coincides with the range of validity of the empirical displacement thickness formula

The form of Eq (4) for the boundary-layer displacement thickness leads to two interesting conclusions. In the present case  $(\delta_1/R) \leq 0.25$ , and hence Eq (4) can be approximated by

$$\delta_1/R \cong gF_2/(1 + 2\gamma\lambda gF_2) \quad (6)$$

and since, for  $(\delta_1/R) < 0.25$ ,  $2\gamma\lambda gF_2 < 0.27$ , it can be seen from Eqs (5) and (6) that

$$\frac{\delta_1}{R} \cong \frac{\theta_w^{2\gamma\lambda-1} x^{\lambda(2\gamma-1)} F_2(p_0, h_0)}{r_t^{2\gamma\lambda}} = \frac{A}{r_t^{2\gamma\lambda}} \quad (7)$$

and

$$\delta_1/R \cong Ar_t^{-0.84}$$

when  $\lambda = 0.3$ ,  $\gamma = 1.4$ . For fixed stagnation conditions the boundary-layer thickness  $\delta_1$  thus varies almost inversely with the throat radius for a conical nozzle of fixed length and divergence angle, provided that  $\delta_1/R$  is sufficiently small

The effective area ratio of a conical nozzle of fixed length and exit area can be increased by decreasing the throat radius  $r_t$ . Now, from the preceding relation between  $\delta_1$  and  $r_t$ , it follows that for a given nozzle and stagnation condition

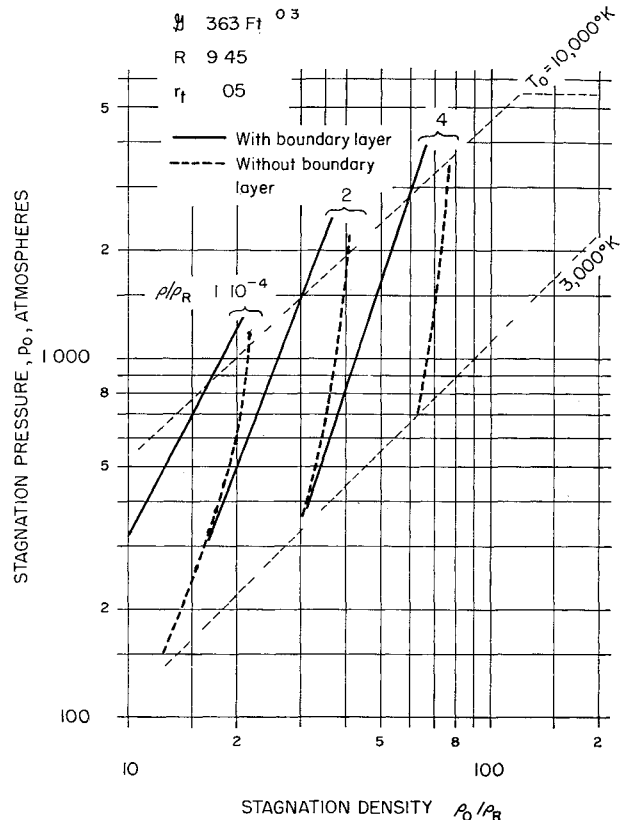


Fig 4 Effect of the boundary layer upon the test section density

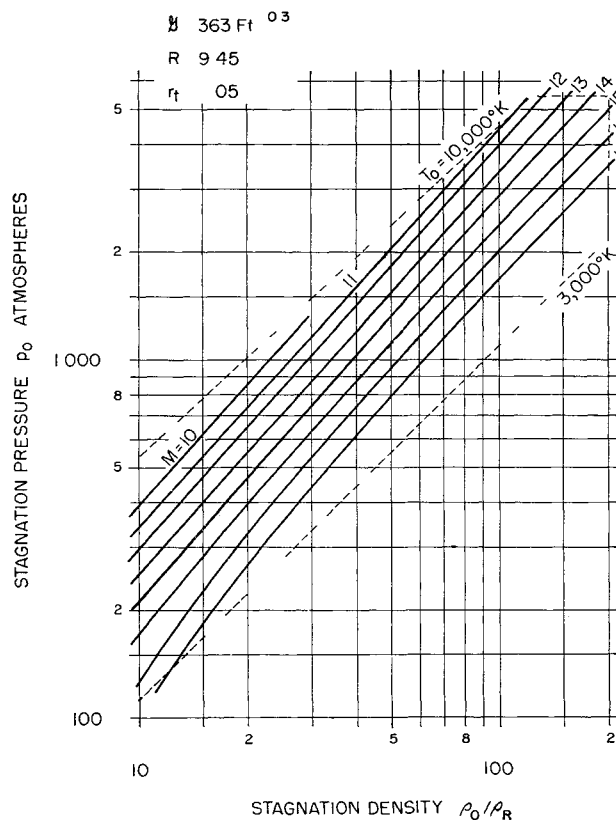


Fig 3 Variation of test section Mach number with stagnation conditions

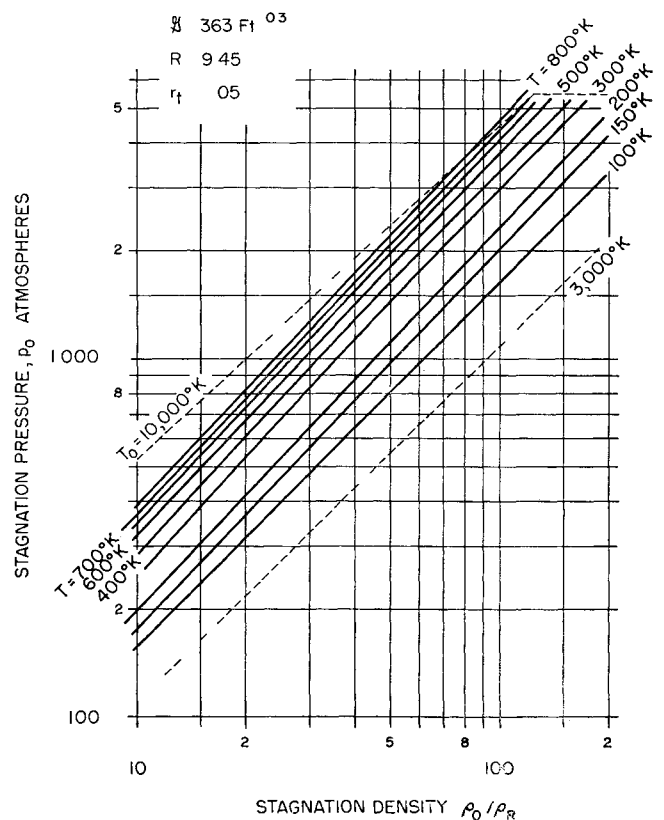


Fig 5 Variation of test section static temperature with stagnation conditions

there must be a critical value of throat radius  $r_t$  such that for  $r_t < r_c$  the effective nozzle area actually decreases with decreasing  $r_t$  because of the rapid boundary-layer growth. This conclusion follows from the expression

$$(A_{eff}/A_t) = (R - \delta_t)^2/r_t^2 = R^2[(1/r_t) - A/(r_t^{2\gamma\lambda} + 1)]^2 \quad (8)$$

which has a maximum value when

$$r_t = r_c = [(2\gamma\lambda + 1)K]^{1/2\gamma\lambda} \quad (9)$$

For example, for the nozzle considered previously when  $p_0 = 4000$  atm,  $h_0/RT_R = 220$ ,  $r_{tc} = 0.0123$  in, and when  $p_0 = 200$  atm,  $h_0/RT_R = 180$ ,  $r_{tc} = 0.0342$  in. At low stagnation pressures the critical throat radius is thus rather close to the actual values used.

**References**

<sup>1</sup> Johnson, R. H., "Hypersonic viscous effects in wind tunnels," *ARS J* **31**, 1022-1024 (1961)  
<sup>2</sup> Burke, A. F. and Bird, K. D., "The use of conical and contoured expansion nozzles in hypervelocity facilities," *Advances in Hypervelocity Techniques* (Plenum Press, New York, 1962), pp 373-424  
<sup>3</sup> Hayes, W. D. and Probst, R. F., *Hypersonic Flow Theory* (Academic Press, New York, 1959), pp 296-298  
<sup>4</sup> Reece, J. W., "Test section conditions generated in the supersonic expansion of real air," *J Aerospace Sci* **29**, 617-618 (1962)  
<sup>5</sup> Sichel, M., "The effect of the boundary layer upon the flow in a conical hypersonic wind tunnel nozzle," Dept. Aeronaut. Astronaut. Eng., Univ. Michigan, Rept. 02953-2-F (July 1963)  
<sup>6</sup> Feldman, S., "Hypersonic gas dynamic charts for equilibrium air," Avco Res. Lab., Res. Rept. 40 (January 1957)  
<sup>7</sup> Goin, K. L., "Mach tables for real gas equilibrium flow of air in hypervelocity test facilities with total temperatures to 10,000°K," Sandia Corp., Rept. SCR-288 (March 1961)  
<sup>8</sup> Blackwell, F., "Properties of argon free air," Ramo-Wooldridge Corp., Los Angeles, Calif., Rept. GM-TR-76 (October 1956)  
<sup>9</sup> Lukasiewicz, J., "An assessment of our present status and further requirements for high temperature hypersonic facilities, round table discussion," Training Center for Exptl. Aerodynamics, Rhode Saint Genese, Belgium, TCEA TM 14 (April 6, 1962)

**Intermolecular-Force Effects on the Thermodynamic Properties of Nitrogen**

C. EDWARD SMITH, JR. \*

Lockheed Missiles and Space Company, Palo Alto, Calif.

**Nomenclature**

- $B$  = second virial coefficient, cm<sup>3</sup>/mole
- $C$  = third virial coefficient, (cm<sup>3</sup>/mole)<sup>2</sup>
- $D$  = fourth virial coefficient, (cm<sup>3</sup>/mole)<sup>3</sup>
- $e$  = internal energy, cal/mole
- $h$  = enthalpy, cal/mole
- $p$  = pressure, atm
- $R$  = gas constant, 1.9872 cal/mole-°K
- $s$  = entropy, cal/mole K
- $T$  = temperature, °K
- $Z$  = compressibility factor
- $\rho$  = density, mole/cm<sup>3</sup>
- $\rho_0$  = reference (or normal) density,  $4.4634 \times 10^{-5}$  mole/cm<sup>3</sup>

Received October 29, 1963. This work was performed as a part of the Lockheed Missiles and Space Company Independent Research Program.

\* Associate Research Scientist, Physical Sciences Laboratory Member AIAA

**Introduction**

KNOWLEDGE of the thermodynamic properties of the working gas is essential to the analysis of data measured in wind tunnels. The present emphasis on high stagnation temperatures, coupled with the widespread usage of nitrogen in hot-shot and shock tunnels, has brought about a comprehensive documentation of the properties of nitrogen.<sup>1-6</sup> Reference 6, in fact, presents calculations of properties up to 100,000°K and includes ionized species up to N<sup>5+</sup>! Neglected in most of these calculations at high temperatures are the equally important high-density effects on thermodynamic properties caused by the intermolecular (or so-called van der Waals) forces.

Although Hilsenrath et al.<sup>1</sup> included intermolecular-force effects, their tables extend to only 100 times normal pressure. The corresponding density ratio is less than 25 for temperatures greater than 1000°K, and the intermolecular-force effects are small. Grabau et al.<sup>7</sup> computed values for much higher densities (up to 300 times normal) but only for the limited temperature range of 3000° to 4000°K.

This paper presents increments in the thermodynamic state variables of nitrogen (based on the virial coefficients of Amdur and Mason<sup>8</sup>) caused by intermolecular forces. These increments in dimensionless form,  $\Delta e/RT$ ,  $\Delta s/R$ , and  $Z$ , are plotted as functions of temperature and logarithm of density ratio. The present results are presented for densities up to 300 times normal at temperatures between 1000° and 9000°K. However, because of dissociation, the accuracy probably is not good above 6000°K.

**Method**

The thermodynamic effects of the intermolecular forces can be included if we express the virial equation of state in powers of density as

$$p = \rho RT(1 + \rho B + \rho^2 C + \rho^3 D) = \rho RTZ \quad (1)$$

where  $B$ ,  $C$ , and  $D$  are virial coefficients and are functions only of temperature. Reference 9 contains equations for the increments in internal energy, enthalpy, and entropy caused by the intermolecular forces. In terms of the virial coefficients, they are

$$\frac{\Delta e}{RT} = - \left[ \rho T \frac{dB}{dT} + \frac{\rho^2}{2} T \frac{dC}{dT} + \frac{\rho^3}{3} T \frac{dD}{dT} \right] \quad (2)$$

$$\frac{\Delta h}{RT} = \frac{\Delta e}{RT} + (Z - 1) \quad (3)$$

and

$$\frac{\Delta s}{R} = - \left\{ \rho T \frac{dB}{dT} + \frac{\rho^2}{2} \left[ B^2 - C + T \frac{dC}{dT} \right] - \frac{\rho^3}{3} \left[ B^3 - 3BC + 2D + T \frac{dD}{dT} \right] \right\} \quad (4)$$

The virial coefficients,  $B$ ,  $C$ , and  $D$ , for nitrogen, tabulated by Amdur and Mason<sup>8</sup> for the temperature range of 1000° to 15,000°K, were used in the present calculations. Since derivatives of the coefficients with respect to temperature are needed in Eqs. (2) and (4), a polynomial representation of each coefficient was computed to facilitate differentiation. A seventh-degree polynomial was fitted by means of the method of least squares through the 24 points for each virial coefficient. In this manner, each coefficient was represented by an equation of the form

$$X(T) = x_0 + x_1 T + x_2 T^2 + \dots + x_7 T^7 \quad (5)$$

where  $T$  is in degrees Kelvin. The curve fitting was done with a digital computer. The polynomial coefficients that were calculated are contained in Table 1. It should be noted that the polynomials fit the values of  $B$ ,  $C$ , and  $D$  over the entire